Nonclassical testosterone signaling through ZIP9 renders melanoma more aggressive in males than in females

Cristina Aguirre-Portolés[1], Riley Payne[2], Aspen Trautz[1], J. Kevin Foskett[2], Christopher A. Natale[1], Todd W. Ridky[1]
[1]Department of Dermatology, [2]Department of Physiology
Perelman School of Medicine, University of Pennsylvania, Philadelphia, PA. USA.

Abstract

Melanoma and most other cancers occur more frequently, and have worse prognosis, in males vs. females. Though sex steroids are thought to be involved, melanoma lacks classical androgen and estrogen receptors. Here we show that testosterone promotes melanoma proliferation by activating ZIP9/SLC39A9, a zinc channel that is not intentionally targeted by any available therapeutics. Testosterone's pro-tumorigenic activity requires zinc influx, MAPK activation and YAP1 nuclear translocation. We demonstrate that inhibitors of the classical androgen receptor (AR), also inhibit ZIP9, and thereby antagonize the pro-tumorigenic effects of testosterone in melanoma. In male mice, AR inhibitors suppressed growth of ZIP9 expressing melanomas, but had no effect on isogenic melanomas lacking ZIP9, nor on melanomas in females. These data suggest that ZIP9 might be effectively targeted in melanoma and other cancers by repurposing modern AR inhibitors, which are currently approved only for prostate cancer.

Introduction

Sex differences in cancer incidence and mortality have been recognized since at least as early as 1949[1], but little progress has been made in understanding the underlying molecular mechanisms for the difference. Cancer incidence and mortality are higher in males than in females in the U.S. and worldwide [2–4]. In the U.S., males are 15% more likely to develop

cancer, and 40% more likely to die of cancer than females. These sex differences are observed in the majority of cancer types from non-reproductive tissues, and remain even after controlling for known risk factors such as environmental and occupational exposures[5]. Despite recent advances in modern targeted and immune therapeutics, which have markedly improved survival for both female and male melanoma patients, females still have more favorable outcomes. Male incidence and rate death for melanoma are 1.6X and 2.5X higher, respectively, in males than in females in the U.S.[2,6]. Defining the mechanisms underlying the broad and persistent sex differences in cancer incidence and outcomes will address a major unresolved question in cancer pathobiology.

We previously showed that estradiol, which circulates at much higher levels in females, inhibits melanoma proliferation in vivo, and tumor growth in vivo. This effect is independent of biologic sex of the tumor, independent of classical estrogen receptors (ER), and results from activation of a nonclassical surface estrogen receptor on melanocytes and melanoma cells called the G Protein Estrogen Receptor (GPER)[7,8]. This work led us to consider whether differences in androgen signaling might also contribute to female vs. male differences in melanoma progression. Testosterone is the most abundant androgen and circulates at much higher levels in males (630 ng/dl) than in females (32 ng/dl)[9]. Testosterone promotes proliferation in vitro in non-gonadal cell types including adipocytes[10], mouse skeletal muscle myoblasts[11], glioblastoma-derived cells[12], lung cancer cell lines[13] and melanoma[14,15]. However, the receptor(s) mediating this activity and the corresponding downstream mechanisms are not defined. Also unknown is whether this androgen activity observed in vitro is relevant to cancer progression in vivo. Here, we define a novel nonclassical testosterone signaling pathway in melanoma that preferentially promotes tumor growth in males, and target this pathway with currently available drugs.

Results and discussion

Melanoma tumors grow more quickly in male vs. female mice.

To test whether preclinical melanoma models recapitulate the female:male survival disparity observed in humans, we first determined growth of human BRAF driven melanoma WM46, ($BRaf^{V600E}$; $CDK4^{R24C}$). Tumors consistently grew faster in male immunodeficient SCID mice compared to matched females, suggesting that the differences were not dependent on T or B cell mediated immune response (Figure 1A). To test whether this phenotype extended to modern genetically engineered preclinical mouse, we used murine YUMM1.7 ($BRaf^{V600E/wt}$;$Pten^{-/-}$$CdkN2a^{-/-}$)[16] in syngeneic immunocompetent C57BL/6 mice. Tumors also consistently grew faster in C57BL/6 male mice compared to matched females (Supplementary Figure 1A).

Testosterone, but not dihydrotestosterone, promotes proliferation in melanoma cells independent of the classical androgen receptor.

Physiological concentrations of testosterone (T) promoted proliferation of both normal early passage primary human melanocytes and melanoma cells (Figure 1B and Supplementary Figure 1B). In contrast, dihydrotestosterone (DHT) had no effect on proliferation of these cell types. This was initially surprising, as DHT has 4-fold increased affinity for the classical nuclear androgen receptor (AR) vs. testosterone, dissociates from AR 3 times slower than T, and is generally considered the more biologically active androgen[17,18]. The proliferative response to testosterone correlated with its concentration and was saturable, strongly suggesting a specific receptor-mediated activity (Figure 1C).

None of the testosterone sensitive primary melanocytes nor melanoma cells we tested express AR (Figure 1D), raising the possibility that a nonclassical hormone receptor is

responsible for the testosterone activity. Recently, the transmembrane zinc transporter SLC39A9/ZIP9 was discovered to bind testosterone in Atlantic Croaker (fish) cells. Importantly, testosterone was determined to have much higher affinity for ZIP9 than either DHT or androstenedione[19]. The human ZIP9 homolog, encoded by the Slc39A9 gene is broadly expressed in most tissues (Supplementary Figure 2A), and we determined that it is expressed in both normal melanocytes and all melanoma lines we have tested to date (Figure 1D and Supplementary Figure 2B). ZIP9 transports zinc (Zn^{++}) across cell and organelle membranes into the cytoplasm and is the only steroid receptor known to directly regulate zinc homeostasis. Zinc is essential for cell differentiation, viability, and proliferation[20,21]. Using the fluorescent zinc-specific probe FluoZin-3, we determined that testosterone induced a rapid increase in cysosolic Zn^{++} in human melanoma cells (Figure 1E). This was followed by a sustained elevation in free cytosolic zinc for at least 2 days in the presence of the androgen (Figure 1F). We next determined that this Zn^{++} influx was necessary for testosterone-induced melanoma cell hyperproliferation, as treatment with the specific Zn^{++} chelator N,N,N′,N′-tetrakis (2-pyridinylmethyl)-1,2-ethanediamine (TPEN), blocked testosterone induced proliferation, while having no significant effect on its own (Figure 1G and Supplementary Figure 3A). Although TPEN has high affinity for zinc, it has also has some ability to chelate copper[22]. To test whether copper flux might contribute to testosterone effects on melanoma proliferation, we treated WM46 cells with copper sulfate, which had no effect on cell proliferation (Supplementary Figure 3B). Moreover, the highly specific copper chelator bathocuproinedisulfonic acid (BCS), did not affect the proliferative response to testosterone, nor did BCS affect testosterone induced Zn^{++} influx (Figure 1H, Supplementary Figure 3C). After determining that Zn^{++} influx was necessary for testosterone induced proliferation, we next questioned whether increased Zn^{++} was sufficient to increase

melanoma proliferation. Exogenous zinc pyrithione, (also a zinc ionophore), and zinc chloride each increased melanoma proliferation (Figure 1I). Other biologically relevant divalent cations, Fe^{++} and Mn^{++}, known to be transported by other ZIP family members[23], had no effect on proliferation (Figure 1I). Together, these results demonstrate that testosterone, but not DHT, promotes melanoma proliferation that is dependent on Zn^{++} influx, and independent of the classic androgen receptor.

ZIP9 mediates testosterone effects in melanoma and promotes tumor growth in vivo. To determine whether ZIP9 is the nonclassical androgen receptor that mediates testosterone effects in melanoma, we used CRISPR-Cas9 and gRNA targeting Slc39A9 exon1 to ablate ZIP9 in human WM46 melanoma and in murine YUMM1.7 melanoma. Isogenic clonal populations of parental ZIP9 expressing (wtZIP9) and ZIP9 null (ΔZIP9) cells were established. ZIP9 protein was completely absent in ΔZIP9 cells (Figure 2A and Supplementary Figure 4A). ΔZIP9 cells did not respond to testosterone, whereas isogenic control clones responded similarly to the parental cells. Consistent with this, ΔZIP9 cells failed to increase cytosolic Zn^{++} following exposure to testosterone or to exogenous zinc salt (Figure 2B and 2C). Therefore, testosterone induces a rapid, ZIP9 dependent, increase in free cytosolic zinc that is required for the hyperproliferation of melanoma-derived cells.

To test whether ZIP9 influences melanoma progression in vivo, WM46 wild-type and isogenic ΔZIP9 cells were subcutaneously injected into the flanks of SCID female and male mice. In female mice, wtZIP9 and ΔZIP9 tumors grew at similar rates. In contrast, wtZIP9 tumors grew much faster than ΔZIP9 tumors in male mice (Figure 2D). The observation that ΔZIP9 tumors in male mice grew at the female rate, suggests that ZIP9 is a major determinant of the male vs. female sex difference in melanoma.

Testosterone induced melanoma proliferation through ZIP9 requires downstream MAPK and YAP1 activation.

Although the studies detailed above show that testosterone promotes melanoma proliferation via ZIP9 dependent Zn^{++} influx, zinc is involved in myriad cellular processes, making it difficult to predict a priori the specific downstream signaling pathways required for the testosterone activity. To start identifying these, we used a 450-element Reverse Phase Protein Array (RPPA) analysis of human WM46 melanoma cells treated with testosterone for 0, 30, 60 and 480 min. While the relative expression of most of the proteins represented on the array was unaffected by testosterone, some were significantly under or overexpressed, including several with known tumor promoting or tumor suppressive functions (Figure 3A, and Supp. Table 1). Downregulated proteins included 14-3-3ε, a tumor suppressor and negative YAP regulator previously implicated in liver, lung, and gastric cancers[24–27], and CDKN2A (p16), a cyclin-dependent kinase (CDK) inhibitor, and one of the most studied tumor suppressors[28]. Upregulated proteins included key elements of tumor promoting pathways, most notably phosphorylated ERK (T202; Y204) and YAP1. Importantly, ΔZIP9 presented decreased basal levels of ERK phosphorylation compared with isogenic wild type clones (Supplementary Figure5A). MAPK activation proved necessary for the hyperproliferative response to testosterone, as the specific ATP-competitive ERK1/2 inhibitor, ulixertinib[29,30] (RVD-523) blocked the testosterone effect, while having no effect on the basal proliferation rate (Figure 3B). Importantly, testosterone-dependent ZIP9 activation renders WM46 cells more dependent on MAPK pathway activation, as viability was compromised when cells were treated with both testosterone and ulixertinib. However,

ΔZIP9 cells treated with both testosterone and ulixertinib proliferated at rates comparable to controls (Figure 3B).

We determined that YAP1 activation is also required for the hyperproliferative response to testosterone. YAP1 is a transcriptional coactivator whose activity is largely regulated by its localization. Testosterone induced rapid YAP1 translocation from cytosol to nucleus in human melanoma cells (Figure 3C and Supplementary Figure 5B). YAP1 subcellular localization is controlled largely by LATS, which phosphorylates YAP1 at Serine 127 and thereby retains YAP1 in the cytosol[31,32]. The YAP inhibitor dobutamine (DOB) also promotes phosphorylation of YAP at Ser127[33]. Consistent with this, testosterone-induced YAP1 nuclear localization and hyperproliferation were both blocked by dobutamine, which had no significant effect on its own (Figure 3C, 3D). Testosterone promotion of YAP1 activity was evidenced by increased expression of a battery of YAP1 target genes including CDC6, CYR61, LATS2 and THBS1 (Figure 3E). Importantly, this testosterone induced expression changes were blocked by dobutamine (Figure 3E). As expected, ΔZIP9 cells were refractory to both testosterone and dobutamine (Supplementary Figure 6A). Basal YAP1 target gene expression was lower in ΔZIP9 cells, suggesting that some degree of constitutive ZIP9 activity (in the absence of testosterone) helps maintain basal YAP signaling (Supplementary Figure 6B).

Pharmacologic ZIP9 blockade inhibits testosterone driven hyperproliferation and melanoma growth in vivo.

Although specific ZIP9 inhibitors are not yet developed, molecular modeling predicts that the FDA approved androgen receptor (AR) inhibitor bicalutamide (BIC) likely competes

with testosterone for ZIP9 binding to the same extracellular pocket and thereby may act as a competitive ZIP9 antagonist[34]. Bicalutamide was developed and approved for prostate cancer, and has now been largely replaced by enzalutamide (ENZ) and apalutamide (APA), which are structurally related analogs with higher affinity for AR, and greater clinical efficacy against advanced prostate cancer[35–39]. While ZIP9 was not known to be an androgen receptor at the time these drugs were developed, we show here that they are nonetheless effective inhibitors of testosterone effects in melanoma cells that lack the originally intended target, AR, but that do express ZIP9. Each compound completely blocked testosterone-induced hyperproliferation, and MAPK activation in several melanoma cells (Figure 4A, 4B, 4C and Supplementary Figure 7A). Importantly, these agents alone had no effect on cell proliferation (Supplementary Figure 7B). Consistent with our working model in which testosterone induced Zn^{++} flux through ZIP9 is the critical mediator of the hyperproliferative response, bicalutamide significantly reduced zinc influx following testosterone exposure (Supplementary Figure 7C). Pharmacologic ZIP9 inhibition with apalutamide also blocked testosterone induction of YAP1 target genes including CDC6, CRIM1 and LATS2 (Supplementary Figure 7D).

Next, we tested whether apalutamide and related analogs inhibit melanoma in vivo. For this, we introduced wtZIP9 or isogenic ΔZIP9 human WM46 melanoma cells (which do not express AR) into SCID mice. Once daily systemically administered apalutamide (20 mg/kg/day via oral gavage) significantly suppressed growth of wtZIP9 tumors in male mice and extended survival (Figure 4D). Similar results were obtained when males were treated with bicalutamide (30mg/kg/day). Importantly, bicalutamide had no effect on wtZIP9 tumors in females (Supplementary Figure 8A). This strongly suggests that the anti-tumor activity

results from inhibition of endogenous androgen signaling through ZIP9. Consistent with this mechanism, bicalutamide also had no effect on ΔZIP9 tumors in male mice (Supplementary Figure 8B).

Together, these data show that nonclassical androgen signaling through ZIP9 promotes melanoma progression in males. As ZIP9 is widely expressed in nearly all tissues, it may be a major determinant of the sex disparity in outcomes for many cancer types (Supplementary Figure 9). The demonstration here that ZIP9 is pharmacologically accessible, suggests that ZIP9 may be a new therapeutic target (Figure 4E), and that currently available AR receptor inhibitors might be useful alone, or in combination with current standard of care therapeutics for a wide range of cancers, especially those arising in males.

Methods

CRISPR-Cas9 mediated ablation of Slc39A9

We used lentiviral transduction to deliver dox-inducible Cas9 and gRNA targeting exon 1 of Slc39A9 in human WM46 and murine YUMM1.7 melanoma cells. Transduced cells were selected with puromycin, and single cells subsequently isolated, expanded and examined for ZIP9 protein expression, compared to clones isolated in parallel in which control gRNA targeted GFP.

The following gRNA sequences were used (5'-3'):

hZIP9_gRNA_Fw caccgTTGGTGGGATGTTACGTGGC

hZIP9_gRNA_Rv aaacGCCACGTAACATCCCACCAAc.

Cell culture and proliferation assays

YUMM1.7 cells were purchased from ATCC (ATCC® CRL-3362™) and cultured in DMEM (Mediatech, Manassas, VA, USA) with 5% FBS (Invitrogen, Carlsbad, CA, USA) and 1% Penicillin-Streptomycin (Thermo Fisher Scientific. # 15140122). WM46 melanoma cells were a gift from Meenhard Herlyn (Wistar Institute, Philadelphia, PA, USA) and were cultured in TU2% media. Tumor cells were regularly tested using MycoAlert Mycoplasma Detection Kit from Lonza (Allendale, NJ, USA). For monitoring cell proliferation $10x10^5$ YUMM1.7 or $15x10^5$ WM46 cells were seed per well in 12-well Cell culture Plates. Cells were treated every second day and manually counted in triplicate using a hemocytometer.

Zinc influx analysis

WM46 cells were loaded with 5 µM FluoZin™-3, AM, cell permeant™ for 20 minutes then incubated in 2 Ca Tyrode's solution (in mM: 140 NaCl, 5 KCl, 1 $MgCl_2$, 2 $CaCl_2$, 10 Glucose and 5 (Na) Pyruvate – pH 7.4) for 5-10 minutes at room temperature prior to imaging. Cells were imaged on a Nikon Ti system using a 20x/0.75 NA objective for fluorescence at 340 nm excitation/515 nm emission (Ca^{2+}-free Fura2 or FluoZin™-3) and 380 nm excitation/515 nm emission (Ca^{2+}-free Fura2 FluoZin™-3). Coverslips were perfused at 1-3 mL/min following this protocol: Ca^{2+} Tyrode's (0-30 secs); Ca^{2+} Tyrode's + DMSO & 5 uM Zinc (30-90 secs); Ca^{2+} Tyrode's + Testosterone & 5uM Zinc (90-360 secs); Ca^{2+} Tyrode's + Testosterone + BIC & 5 uM Zn (360-470 secs); Ca^{2+} Tyrode's washout (470-500 secs). 100 milliseconds exposure images for each wavelength were collected every 2 seconds. For analyzing the long-term consequences of testosterone treatment, cells were treated with the androgen for 96 hours prior to the Zinc influx study. FluoZin™-3, AM, cell permeant™ zinc specific indicator was used following the manufacturer recommendations (Thermo Fisher

Scientifics, # F24195). Cells were incubated with FluoZin™-3 following manufacturer recommendation and exposed to 400nM Zn pyrithione or $ZnCl_2$. Images were acquired with EVOS BLA. Fluorescence was quantitated using ImageJ (National Institutes of Health, Bethesda, MD, USA), and statistical analysis was performed using Graphpad Prism software.

Western blot, immunofluorescence and antibodies

Adherent cells were washed once with PBS and lysed with 8M urea containing 50mM NaCl and 50mM Tris-HCl, pH 8.3, 10mM dithiothreitol, 50mM iodoacetamide. Lysates were quantified (Bradford assay), normalized, reduced, and resolved by SDS gel electrophoresis on 4–15% Tris/Glycine gels (Bio-Rad, Hercules, CA, USA). Resolved protein was transferred to PVDF membranes (Millipore, Billerica, MA, USA) using a Semi-Dry Transfer Cell (Bio-Rad), blocked in 5% BSA in TBS-T and probed with primary antibodies recognizing β-Actin (Cell Signaling Technology, #3700. 1:4000, Danvers, MA, USA), ZIP9 (Cell Signaling Technology, #137205, 1:500), P-ERK (Cell Signaling Technology, Phospho-p44/42 MAPK (Erk1/2) (Thr202/Tyr204) (D13.14.4E) XP® Rabbit mAb #4370. 1:1000), ERK (Cell Signaling Technology, p44/42 MAPK (Erk1/2) (137F5) Rabbit mAb #4695, 1:1000), P-RB (Cell Signaling Technology, Phospho-Rb (Ser807/811) (D20B12) XP® Rabbit mAb #8516, 1:1000), and RB (Cell Signaling Technology, Rb (D20) Rabbit mAb #9313. 1:1000). After incubation with the appropriate secondary antibody (Rabbit Anti-Mouse IgG H&L (Biotin) preabsorbed (ab7074); Anti-mouse IgG, HRP-linked Antibody #7076. 1:2000) proteins were detected using ClarityTM Western ECL Substrate (Bio-Rad. #170-5060). All western blots were repeated at least 3 times. To monitor YAP1 nuclear translocation by Western blot analysis, nuclear fractionation was performed using protein lysis buffer containing 10nM HEPES, 1mM KCl, 1.5mM MgCl2 and 10%Glycerol (Buffer

A). After washing the adherent cells with DPBS, samples were resuspended in Buffer A and incubated for 5 minutes in ice in the presence of 0.1% Triton-X-100. After centrifugation, the nuclear fraction remained as a pellet while the supernatant corresponded to the cytosolic fraction. Nuclear fraction was washed with Buffer A. After centrifugation, the nuclear fraction was resuspended in RIPA buffer and samples were boiled for 5 minutes prior sample loading. Cytosolic fraction was centrifuged during 15 min at 13500 rpm. Only the supernatant was kept after centrifugation. Western blot was performed as described before and the following antibodies were used for protein detection: β-tubulin (Cell Signaling Technology, β-Tubulin (9F3) Rabbit mAb #2128. 1:1000), PARP (Cell Signaling Technology, Rabbit mAb #9542. 1:1000), YAP1 (Cell Signaling Technology, YAP (D8H1X) XP® Rabbit mAb #14074. 1:1000). For immunofluorescence in adherent cells, samples were fixed with 4% Paraformaldehyde (Affymetrix; #19943) for 7 minutes and permeabilized with iced-cold methanol. After blocking with 10%FBS:0.03%Triton-X100, primary antibodies were incubated overnight in blocking solution (β-Actin and YAP1 antibodies detailed above). After three washes in DPBS:0.03%Triton X-100) cells were incubated with secondary antibodies for 45 minutes at room temperature (Goat anti-Mouse IgG (H+L) Highly Cross-Adsorbed Secondary Antibody, Alexa Fluor 594. Goat anti-Rabbit IgG (H+L) Highly Cross-Adsorbed Secondary Antibody, Alexa Fluor 488). Cells were rinsed with PBS-Triton 0.03% three times and coverslips were mounted with ProLong Gold antifade reagent with DAPI (#P36935; Thermo Fisher Scientific). Images were captured using a Leica DM IL microscope and registered using LAS software. For fluorescence intensity quantification ImageJ software (National Institutes of Health, Bethesda, MD, USA) was used, and statistical analysis was performed with GraphPad Prism software.

Mice, subcutaneous tumors and pharmacologic treatments

All mice were purchased from Taconic Biosciences, Inc. (Rensselaer, NY, USA). Six to eight week old male and female C57BL/6NTac or IcrTac:ICR-Prkdcscid were allowed to reach sexually mature ages or to acclimatize for one week prior to being used for experiments. These studies were performed without inclusion/exclusion criteria or blinding but included randomization. Based on a twofold-anticipated effect, we performed experiments with at least 5 biological replicates. All procedures were performed in accordance with International Animal Care and Use Committee (IACUC)-approved protocols at the University of Pennsylvania. Subcutaneous tumors were initiated by injecting tumor cells in 50% Matrigel (Corning, Bedford, MA, USA) into the subcutaneous space on the right flanks of mice. 10 x 10^6 human WM46 cells were used for each tumor. Oral administration of vehicle, bicalutamide (30mg/kg/day) or apalutamide (20mg/kg/day) was performed daily. 100 µl of drug were administrated by oral gavage [10%DMSO:90%Vehicle (15% ethanol:85% sesame oil)]. Weight and health status of the mice as well as tumor growth were monitored daily. As subcutaneous tumors grew in mice, perpendicular tumor diameters were measured using calipers. Volume was calculated using the formula L × W^2 × 0.52, where L is the longest dimension and W is the perpendicular dimension. Animals were euthanized when tumors exceeded a protocol-specified size of 15 mm in the longest dimension. Secondary endpoints include severe ulceration, death, and any other condition that falls within the IACUC guidelines for Rodent Tumor and Cancer Models at the University of Pennsylvania.

Quantitative RT-PCR

RNA was extracted using RNeasy kit (Qiagen. #74104) following the manufacturer's instructions. cDNA was obtained using High Capacity cDNA Reverse Transcription Kit (Applied Biosystems #4368814). For quantitative real-time PCR, PowerUP™ SYBR™ Green Master Mix (Applied Biosystems #A25741) was used. ViiA 7 Real-Time PCR System was used to perform the reaction (Applied Biosystems). Values were corrected by actin expression. The $2^{-\Delta\Delta Ct}$ method was applied to calculate the relative gene expression. Primers used for the amplification are included in Supplementary Table 2.

Statistical analysis

To optimize scientific rigor, each experiment included at least n=5 replicates, which will provide 100% power to detect at least a 50% difference between groups with 95% confidence. For experiments comparing two groups (treated vs control), significance was calculated using the Mann-Whitney test. For experiments with more than two groups, one-way ANOVA with Tukey's honest significance difference test was performed. Statistical analyses were performed using Graphpad Prism Software.

P-values and significance: n.s. $p > 0.05$; *$p < 0.05$; **$p < 0.01$; ***$p < 0.001$; ****$p < 0.0001$.

Acknowledgements

The authors thank the University of Pennsylvania Skin Biology and Disease Research-based center for analysis of tissue sections. T.W.R. is supported by a grants from the NIH/NCI (R01 CA163566, R41CA228695), and by the Stiefel award from the Dermatology Foundation. This work was also supported in part by the Penn Skin Biology and Diseases Resource-based Center (P30-AR069589).

Figure legends

Figure 1: Biologic sex and testosterone influence melanoma proliferation A. Tumor growth in SCID male and female mice bearing human melanoma derived tumors (WM46). Five mice per condition. Error bars represent standard error of the mean (SEM). **B.** Relative cell proliferation determined after 6 days of treatment with vehicle (DMSO), 100 nM testosterone (T) or 100 nM dihydrotestosterone (DHT). Human melanocytes (H.Mel.), WM46 human melanoma cells are shown. The graphs represent the average of three independent experiments. Error bars represent standard error of the mean (SEM). **C.** Relative cell proliferation of WM46 cells exposed to increasing concentrations of testosterone (T). **D.** AR and ZIP9 protein expression by Western blot. Human primary melanocytes, WM46, YUMM1.7 and human uveal melanoma (Mel.290) cells are shown. MCF7 breast cells was used as positive control for AR expression. **E.** Time-lapse analysis of Zn^{++} influx upon testosterone addition. FluoZin-3 was used as Zn^{++} reporter. **F.** Intracellular levels of Zinc after long-term testosterone treatment. **G.** WM46 relative proliferation in the presence of Zinc chelator (TPEN). **H.** WM46 relative proliferation in the presence of copper chelator (BCS). **I.** WM46 relative proliferation in the presence Zinc salts, $FeSO_4$ and $MnCl_2$.
**** p value<0.0001; *** p value<0.001; ** p value<0.005; * p value<0.01.

Figure 2: ZIP9 mediates testosterone effects in melanoma. A. Relative cell proliferation in clonal populations of WM46 wtZIP9 and ΔZIP9 exposed to increasing concentrations of testosterone (T) in vitro. The graph represents the average of three independent experiments. Error bars represent standard error of the mean (SEM). **B.** Intracellular levels of Zinc in human melanoma ΔZIP9 cells. Graphs represent the average of three independent

experiments. Error bars represent standard error of the mean (SEM). **C.** Relative cell proliferation in the presence of T, Zinc chelator (TPEN) and $ZnCl_2$. The graph represents the average of three independent experiments. Error bars represent standard error of the mean (SEM). **D.** WM46 derived subcutaneous tumor growth in SCID male and female mice (wtZIP9 and ΔZIP9). **** p value<0.0001; ** p value<0.005; * p value<0.01.

Figure 3: Testosterone induced melanoma hyperproliferation requires ZIP9 and activation of MAPK and YAP1. A. RPPA analysis displaying changes in protein expression in WM46 human melanoma cells following exposure to T. Down-regulated proteins are shown in green; Up-regulated proteins in light red. Control proteins showing no fold-change when compared to vehicle-treated cells are shown in blue. **B.** Relative cell proliferation under pharmacologic ERK1/2 inhibition with 50nM RVD-523 (ERKi) alone or in combination with testosterone. wtZIP9 and DZIP9 WM46 cells are shown. Western blot shows levels of phosphorylation of the ERK target RSK in wtZIP9 and DZIP9 WM46 cells. **C.** YAP1 immunodetection after 30 minutes of exposure to testosterone (T) and/or dobutamine (DOB). YAP1 is shown in green; b-actin is shown in red; DAPI marks DNA in blue. Scale bar=25mm. **D.** Relative cell proliferation of wtZIP9 and DZIP9 WM46 cells after treatment with testosterone (T) and/or dobutamine (DOB). **E.** Relative mRNA expression of YAP1 and a battery of YAP1 target genes after 24 hours in the presence of testosterone and/or dobutamine. **** p value<0.0001; *** p value<0.001, ** p value<0.005; * p value<0.01.

Figure 4: Pharmacologic ZIP9 blockade inhibits melanoma in vivo. A. Relative cell proliferation in human-derived melanoma cells (WM46) in the presences of testosterone (T) and/or AR inhibitors (BIC:Bicalutamide; ENZ:Enzalutamide; APA:Apalutamide). Western blot showing protein levels in WM46 cells treated with testosterone, BIC and Zinc chelator

(TPEN). **B.** Relative cell proliferation in human and murine derived melanoma cells treated with T in combination with Apalutamide. **C.** Relative cell proliferation of WM46 wtZIP9 cells and ΔZIP9 cells in the presence of T and APA. **D.** Tumor growth in SCID male mice bearing WM46 derived subcutaneous tumors (APA treatment: 20mg/kg/day via oral gavage). **E.** ZIP9 activation promotes ERK phosphorylation and induces YAP1 nuclear translocation. AR inhibitors [represented in the figure by apalutamide (APA)] block testosterone effects through ZIP9 inactivation.

Figure 1

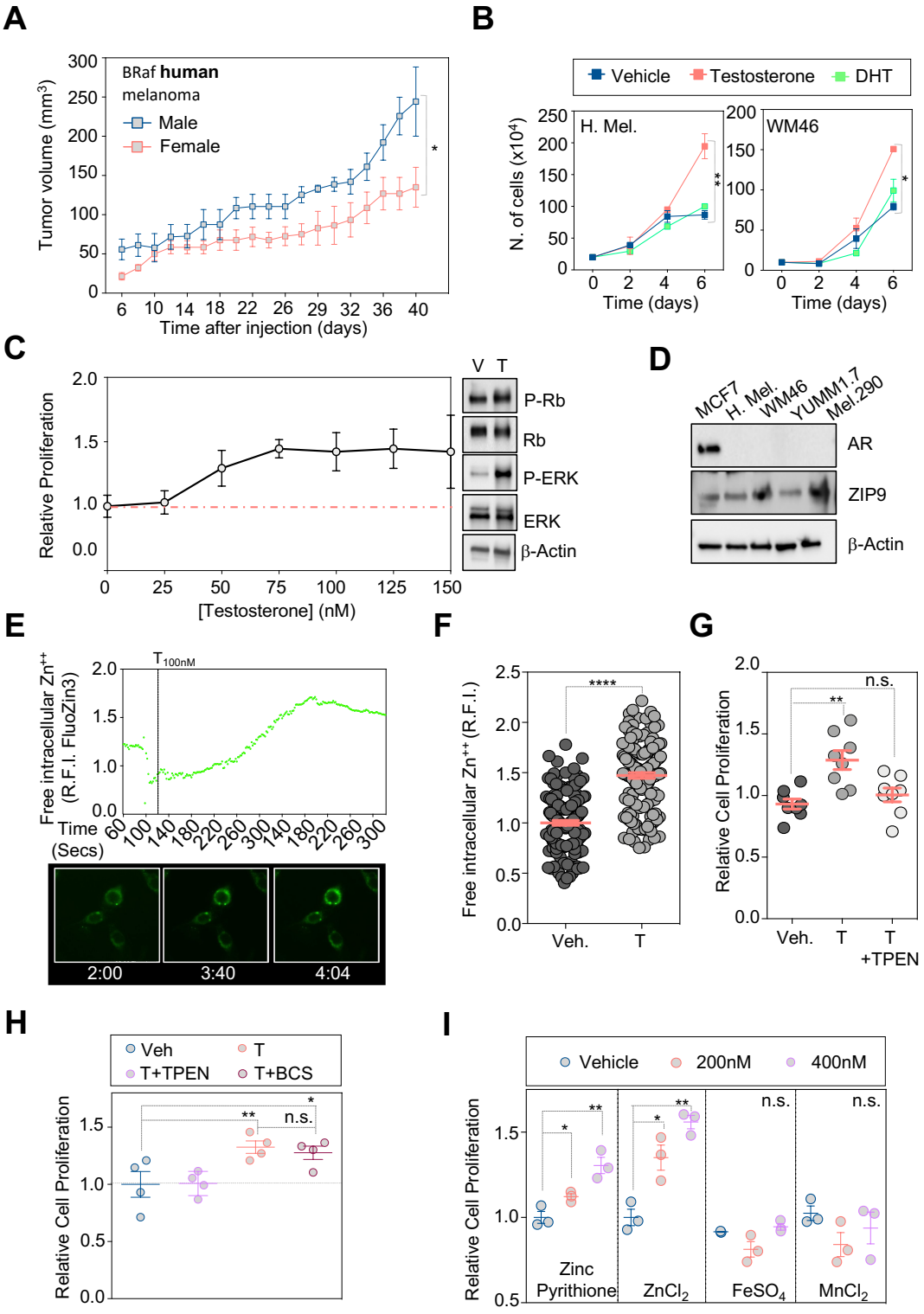
A
BRaf human melanoma
Male
Female
Tumor volume (mm3)
Time after injection (days)
B
Vehicle
Testosterone
DHT
H. Mel.
WM46
N. of cells (x10^4)
Time (days)
C
V T
P-Rb
Rb
P-ERK
ERK
β-Actin
Relative Proliferation
[Testosterone] (nM)
D
MCF7
H. Mel.
WM46
YUMM1.7
Mel.290
AR
ZIP9
β-Actin
E
T100nM
Free intracellular Zn++ (R.F.I. FluoZin3)
Time (Secs)
2:00
3:40
4:04
F
Free intracellular Zn++ (R.F.I.)
Veh.
T
G
Relative Cell Proliferation
n.s.
Veh.
T
T +TPEN
H
Veh
T
T+TPEN
T+BCS
Relative Cell Proliferation
n.s.
I
Vehicle
200nM
400nM
Relative Cell Proliferation
n.s.
Zinc Pyrithione
ZnCl2
FeSO4
MnCl2

Figure 2

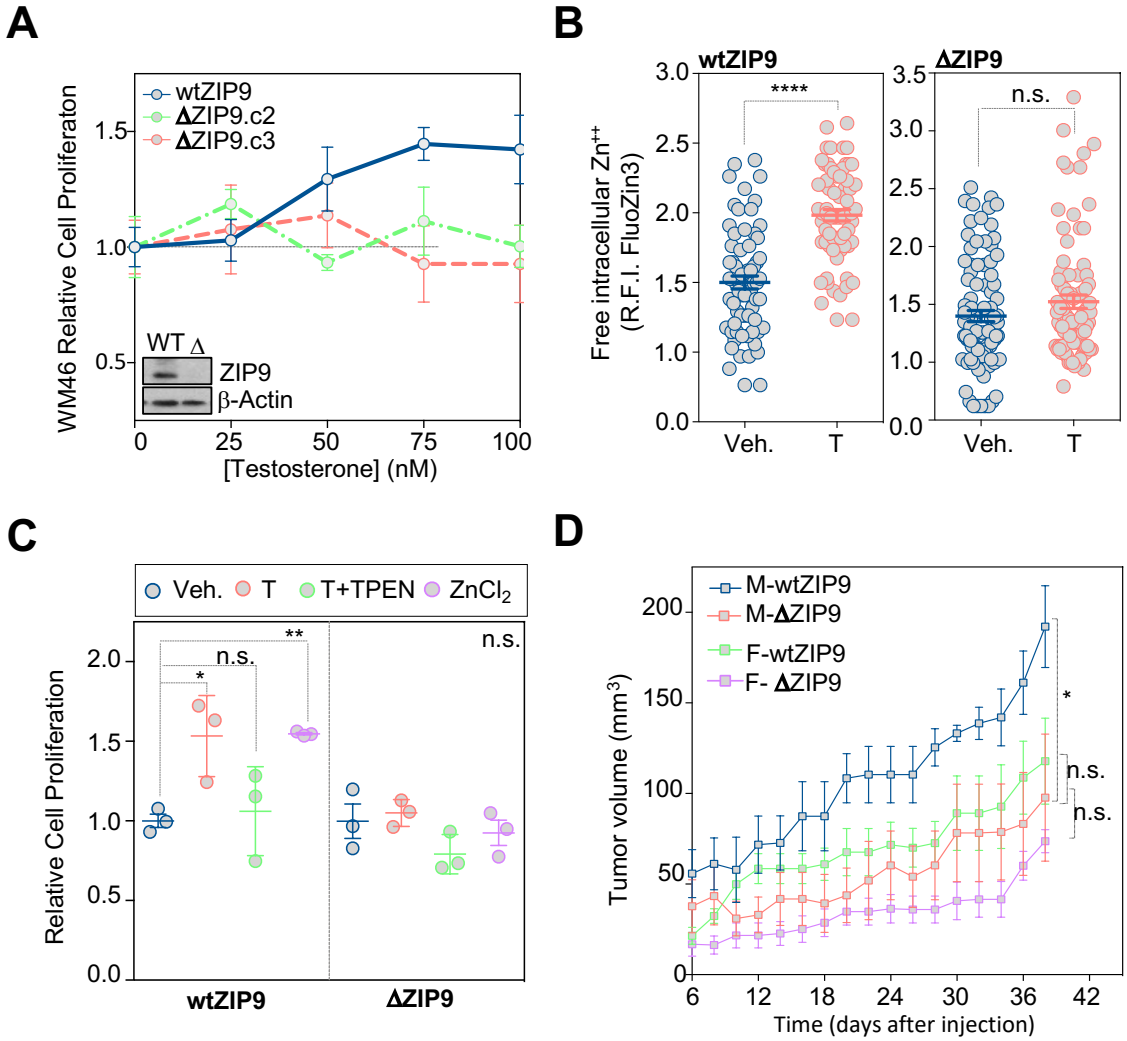
A
wtZIP9
ΔZIP9.c2
ΔZIP9.c3
WM46 Relative Cell Proliferaton
1.5
1.0
0.5
WT Δ
ZIP9
β-Actin
0
25
50
75
100
[Testosterone] (nM)
B
wtZIP9
ΔZIP9
Free intracellular Zn++
(R.F.I. FluoZin3)
3.0
2.5
2.0
1.5
1.0
0.0
****
n.s.
Veh.
T
C
Veh.
T
T+TPEN
ZnCl2
Relative Cell Proliferation
2.0
1.5
1.0
0.5
0.0
n.s.
*
**
n.s.
wtZIP9
ΔZIP9
D
M-wtZIP9
M-ΔZIP9
F-wtZIP9
F- ΔZIP9
Tumor volume (mm3)
200
150
100
50
0
*
n.s.
n.s.
6
12
18
24
30
36
42
Time (days after injection)

Figure 3

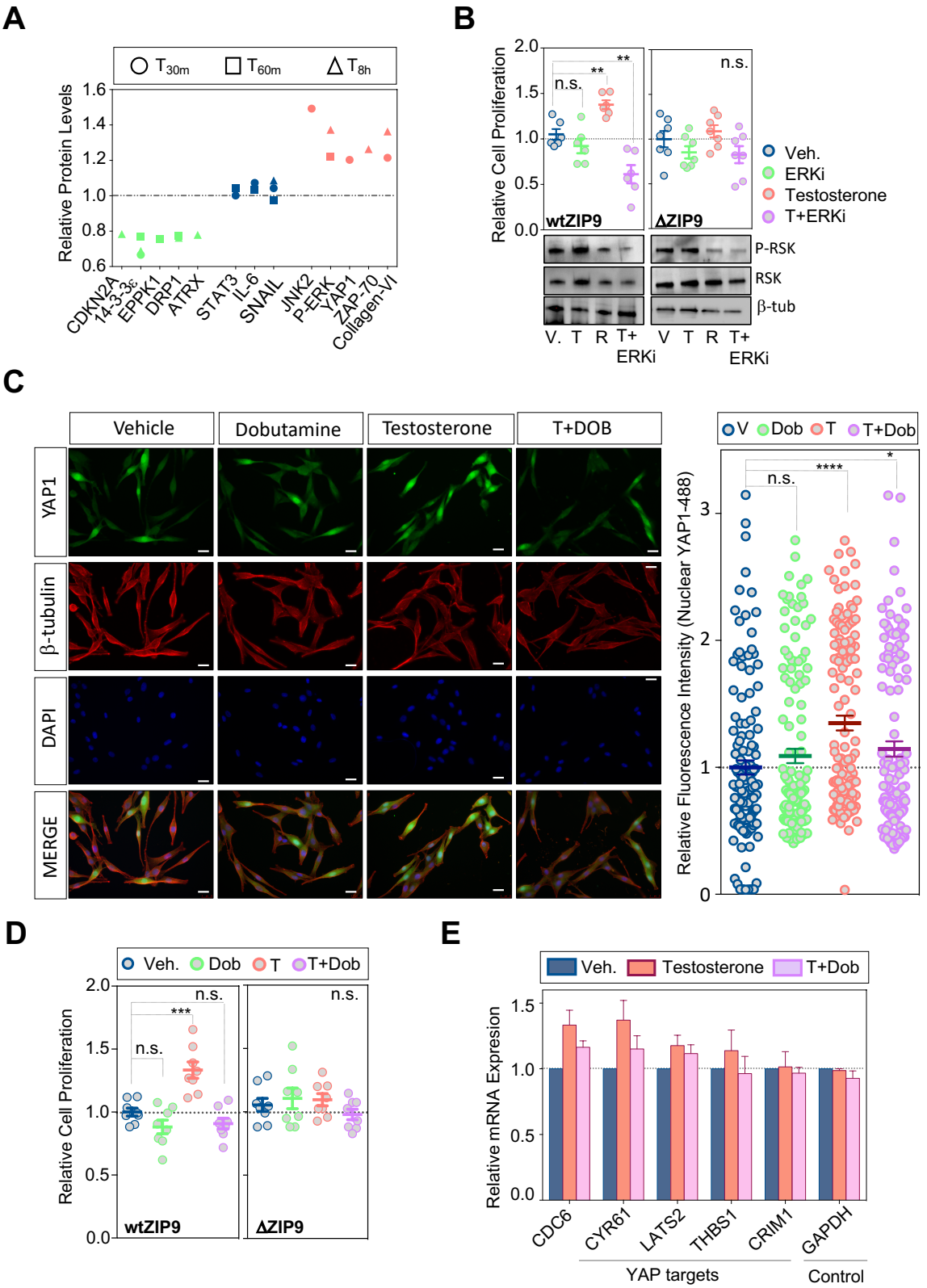
A
T30m
T60m
T8h
Relative Protein Levels
1.6
1.4
1.2
1.0
0.8
0.6
CDKN2A
14-3-3ε
EPPK1
DRP1
ATRX
STAT3
IL-6
SNAIL
JNK2
P-ERK
YAP1
ZAP-70
Collagen-VI
B
Relative Cell Proliferation
2.0
1.5
1.0
0.5
0.0
n.s.
**
**
n.s.
wtZIP9
ΔZIP9
Veh.
ERKi
Testosterone
T+ERKi
P-RSK
RSK
β-tub
V. T R T+ ERKi
V T R T+ ERKi
C
Vehicle
Dobutamine
Testosterone
T+DOB
YAP1
β-tubulin
DAPI
MERGE
V Dob T T+Dob
Relative Fluorescence Intensity (Nuclear YAP1-488)
3
2
1
0
n.s.
****
*
D
Veh. Dob T T+Dob
Relative Cell Proliferation
2.0
1.5
1.0
0.5
0.0
n.s.
***
n.s.
n.s.
wtZIP9
ΔZIP9
E
Veh. Testosterone T+Dob
Relative mRNA Expresion
1.5
1.0
0.5
0.0
CDC6
CYR61
LATS2
THBS1
CRIM1
GAPDH
YAP targets
Control

Figure 4

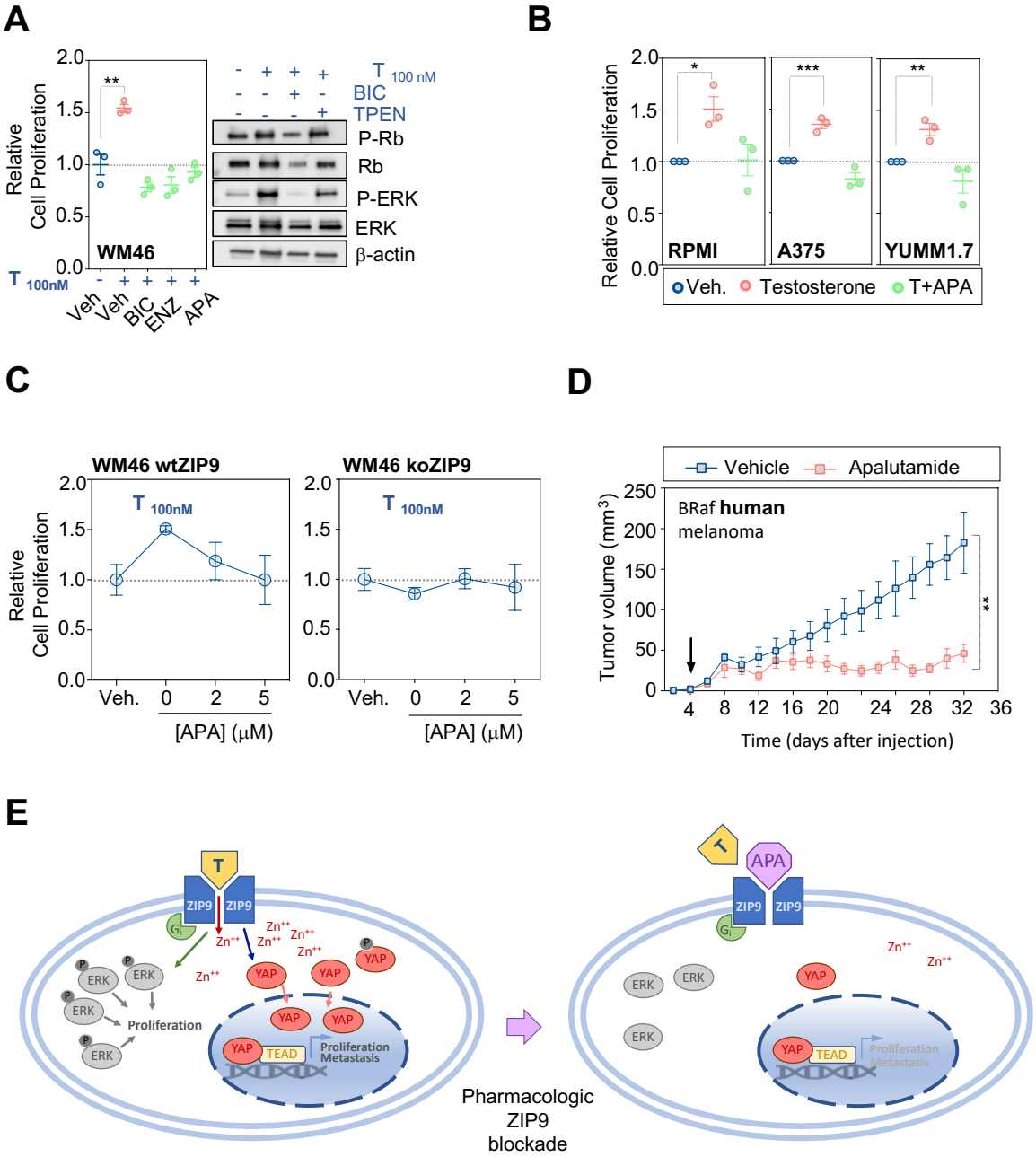

A
Relative Cell Proliferation
WM46
T 100nM
Veh
Veh
BIC
ENZ
APA
T 100 nM
BIC
TPEN
P-Rb
Rb
P-ERK
ERK
β-actin
B
Relative Cell Proliferation
RPMI
A375
YUMM1.7
Veh.
Testosterone
T+APA
C
WM46 wtZIP9
WM46 koZIP9
T 100nM
Relative Cell Proliferation
Veh.
[APA] (μM)
D
Vehicle
Apalutamide
BRaf human melanoma
Tumor volume (mm3)
Time (days after injection)
E
T
ZIP9
Gi
Zn++
YAP
ERK
Proliferation
TEAD
Proliferation Metastasis
APA
Pharmacologic ZIP9 blockade

References

1. Clemmesen, J. & Busk, T. Cancer Mortality Among Males and Females in Denmark, England, and Switzerland: V. Incidence of Accessible and Inaccessible Cancers in Danish Towns and Rural Areas. *Cancer Res* **9**, 415–421 (1949).
2. Surveillance, Epidemiology, and End Results Program. *SEER* https://seer.cancer.gov/index.html.
3. GLOBOCAN2018. https://bit.ly/2Vd3C6a.
4. Siegel, R. L., Miller, K. D. & Jemal, A. Cancer statistics, 2020. *CA Cancer J Clin* **70**, 7–30 (2020).
5. Edgren, G., Liang, L., Adami, H.-O. & Chang, E. T. Enigmatic sex disparities in cancer incidence. *Eur. J. Epidemiol.* **27**, 187–196 (2012).
6. Hieken, T. J. *et al.* Sex-Based Differences in Melanoma Survival in a Contemporary Patient Cohort. *Journal of Women's Health* (2020) doi:10.1089/jwh.2019.7851.
7. Natale, C. A. *et al.* Activation of G protein-coupled estrogen receptor signaling inhibits melanoma and improves response to immune checkpoint blockade. *Elife* **7**, (2018).
8. Natale, C. A. *et al.* Sex steroids regulate skin pigmentation through nonclassical membrane-bound receptors. *Elife* **5**, (2016).
9. Sperling, M. A. *Pediatric Endocrinology-Mean Sex Steriod Concentration in Infants, Children and adults.* (Elsevier Health Sciences, 2014).
10. Barbosa-Desongles, A., Hernández, C., Simó, R. & Selva, D. M. Testosterone induces cell proliferation and cell cycle gene overexpression in human visceral preadipocytes. *Am. J. Physiol., Cell Physiol.* **305**, C355-359 (2013).
11. Fu, R. *et al.* Novel evidence that testosterone promotes cell proliferation and differentiation via G protein-coupled receptors in the rat L6 skeletal muscle myoblast cell line. *J. Cell. Physiol.* **227**, 98–107 (2012).
12. Rodríguez-Lozano, D. C., Piña-Medina, A. G., Hansberg-Pastor, V., Bello-Alvarez, C. & Camacho-Arroyo, I. Testosterone Promotes Glioblastoma Cell Proliferation, Migration, and Invasion Through Androgen Receptor Activation. *Front. Endocrinol.* **10**, (2019).
13. Maasberg, M. *et al.* Androgen receptors, androgen-dependent proliferation, and 5 alpha-reductase activity of small-cell lung cancer cell lines. *Int. J. Cancer* **43**, 685–691 (1989).
14. Mather, J. P. & Sato, G. H. The growth of mouse melanoma cells in hormone-supplemented, serum-free medium. *Experimental Cell Research* **120**, 191–200 (1979).
15. Allil, P. A. A., Visconti, M. A. & Isoldi, A. M. L. C. and M. C. Photoperiod and Testosterone Modulate Growth and Melanogenesis of S91 Murine Melanoma. *Medicinal Chemistry* http://www.eurekaselect.com/82341/article (2008).
16. Meeth, K., Wang, J. X., Micevic, G., Damsky, W. & Bosenberg, M. W. The YUMM lines: a series of congenic mouse melanoma cell lines with defined genetic alterations. *Pigment Cell Melanoma Res* **29**, 590–597 (2016).
17. Askew, E. B., Gampe, R. T., Stanley, T. B., Faggart, J. L. & Wilson, E. M. Modulation of Androgen Receptor Activation Function 2 by Testosterone and Dihydrotestosterone. *J. Biol. Chem.* **282**, 25801–25816 (2007).
18. Tóth, M. & Zakár, T. Relative binding affinities of testosterone, 19-nortestosterone and their 5α-reduced derivatives to the androgen receptor and to other androgen-binding proteins: a suggested role of 5α-reductive steroid metabolism in the dissociation of

"myotropic" and "androgenic" activities of 19-nortestosterone. *Journal of Steroid Biochemistry* **17**, 653–660 (1982).
19. Berg, A. H., Rice, C. D., Rahman, M. S., Dong, J. & Thomas, P. Identification and characterization of membrane androgen receptors in the ZIP9 zinc transporter subfamily: I. Discovery in female atlantic croaker and evidence ZIP9 mediates testosterone-induced apoptosis of ovarian follicle cells. *Endocrinology* **155**, 4237–4249 (2014).
20. Beyersmann, D. & Haase, H. Functions of zinc in signaling, proliferation and differentiation of mammalian cells. *Biometals* **14**, 331–341 (2001).
21. Lo, M. N., Damon, L. J., Wei Tay, J., Jia, S. & Palmer, A. E. Single cell analysis reveals multiple requirements for zinc in the mammalian cell cycle. *Elife* **9**, (2020).
22. Fatfat, M. *et al.* Copper chelation selectively kills colon cancer cells through redox cycling and generation of reactive oxygen species. *BMC Cancer* **14**, 527 (2014).
23. He, L. *et al.* ZIP8, member of the solute-carrier-39 (SLC39) metal-transporter family: characterization of transporter properties. *Mol. Pharmacol.* **70**, 171–180 (2006).
24. Fu, H., Subramanian, R. R. & Masters, S. C. 14-3-3 proteins: structure, function, and regulation. *Annu. Rev. Pharmacol. Toxicol.* **40**, 617–647 (2000).
25. Lee, C.-L. *et al.* Strategic shotgun proteomics approach for efficient construction of an expression map of targeted protein families in hepatoma cell lines. *Proteomics* **3**, 2472–2486 (2003).
26. Seow, T. K. *et al.* Two-dimensional electrophoresis map of the human hepatocellular carcinoma cell line, HCC-M, and identification of the separated proteins by mass spectrometry. *Electrophoresis* **21**, 1787–1813 (2000).
27. Leal, M. F. *et al.* Clinical implication of 14-3-3 epsilon expression in gastric cancer. *World J. Gastroenterol.* **18**, 1531–1537 (2012).
28. Ruas, M. & Peters, G. The p16INK4a/CDKN2A tumor suppressor and its relatives. *Biochim. Biophys. Acta* **1378**, F115-177 (1998).
29. Germann, U. A. *et al.* Targeting the MAPK Signaling Pathway in Cancer: Promising Preclinical Activity with the Novel Selective ERK1/2 Inhibitor BVD-523 (Ulixertinib). *Mol. Cancer Ther.* **16**, 2351–2363 (2017).
30. Mendzelevski, B. *et al.* Effect of ulixertinib, a novel ERK1/2 inhibitor, on the QT/QTc interval in patients with advanced solid tumor malignancies. *Cancer Chemother. Pharmacol.* **81**, 1129–1141 (2018).
31. Zhao, B., Li, L., Tumaneng, K., Wang, C.-Y. & Guan, K.-L. A coordinated phosphorylation by Lats and CK1 regulates YAP stability through SCFβ-TRCP. *Genes Dev* **24**, 72–85 (2010).
32. Zhao, B. *et al.* Inactivation of YAP oncoprotein by the Hippo pathway is involved in cell contact inhibition and tissue growth control. *Genes Dev* **21**, 2747–2761 (2007).
33. Fujii, M. Exploration of a new drug that targets YAP. *J. Biochem.* **152**, 209–211 (2012).
34. Bulldan, A., Malviya, V. N., Upmanyu, N., Konrad, L. & Scheiner-Bobis, G. Testosterone/bicalutamide antagonism at the predicted extracellular androgen binding site of ZIP9. *Biochim Biophys Acta Mol Cell Res* **1864**, 2402–2414 (2017).
35. Tran, C. *et al.* Development of a second-generation antiandrogen for treatment of advanced prostate cancer. *Science* **324**, 787–790 (2009).
36. Lam, H.-M. *et al.* Durable Response of Enzalutamide-resistant Prostate Cancer to Supraphysiological Testosterone Is Associated with a Multifaceted Growth Suppression and Impaired DNA Damage Response Transcriptomic Program in Patient-derived

Xenografts. *Eur. Urol.* (2019) doi:10.1016/j.eururo.2019.05.042.
37. Ponnusamy, S. *et al.* Orally-Bioavailable Androgen Receptor Degrader, A Potential Next-Generation Therapeutic for Enzalutamide-Resistant Prostate Cancer. *Clin. Cancer Res.* (2019) doi:10.1158/1078-0432.CCR-19-1458.
38. Teply, B. A. *et al.* Bipolar androgen therapy in men with metastatic castration-resistant prostate cancer after progression on enzalutamide: an open-label, phase 2, multicohort study. *Lancet Oncol.* **19**, 76–86 (2018).
39. Chi, K. N. *et al.* Apalutamide for Metastatic, Castration-Sensitive Prostate Cancer. *N. Engl. J. Med.* **381**, 13–24 (2019).